Citation Format:

Memeo, Roberto, et al. "Automatic imaging of Drosophila embryos with light sheet fluorescence microscopy on chip." *Journal of Biophotonics* 14.3 (2021): e202000396.

DOI link:

https://doi.org/10.1002/jbio.202000396

FULL ARTICLE

Automatic imaging of *Drosophila* embryos with Light Sheet Fluorescence Microscopy on chip

Roberto Memeo,[1,2,†] Petra Paiè,*[2,†] Federico Sala,[1,2] Michele Castriotta,[1,2] Chiara Guercio,[3] Thomas Vaccari,[3] Roberto Osellame,[2,1] Andrea Bassi[1,2] and Francesca Bragheri[2]

1 Dipartimento di Fisica-Politecnico di Milano, Piazza Leonardo da Vinci 32, 20133 Milan, Italy.

2 Istituto di Fotonica e Nanotecnologie (IFN)-CNR, Piazza Leonardo da Vinci 32, 20133 Milan, Italy.

3 Dipartimento di Bioscienze, Università degli Studi di Milano, via Celoria 26, 20133 Milan, Italy.

*** Correspondence**

Petra Paiè Istituto di Fotonica e Nanotecnologie (IFN)-CNR, Piazza Leonardo da Vinci 32, 20133 Milan, Italy.

Email: petra.paie@cnr.it

We present a microscope on chip for automated imaging of *Drosophila* embryos by light sheet fluorescence microscopy. This integrated device, constituted by both optical and microfluidic components, allows the automatic acquisition of a 3D stack of images for specimens diluted in a liquid suspension. The device has been fully optimized to address the challenges related to the specimens under investigation. Indeed, the thickness and the high ellipticity of *Drosophila* embryos can degrade the image quality. In this regard, optical and fluidic optimization have been carried out to implement dual-sided illumination and automatic sample orientation. In addition, we highlight the dual color investigation capabilities of this device, by processing two sample populations encoding different fluorescent proteins. This work was made possible by the versatility of the used fabrication technique, femtosecond laser micromachining, which allows straightforward fabrication of both optical and fluidic components in glass substrates.

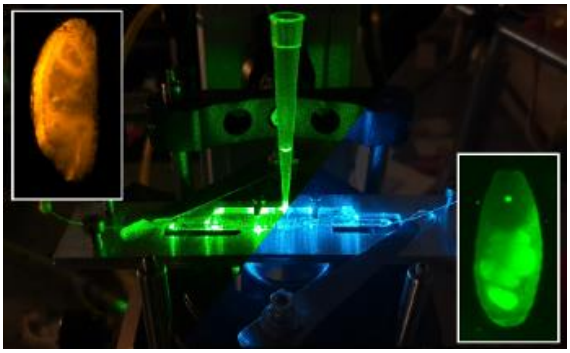

KEYWORDS

Light sheet fluorescence microscopy, 3D imaging, lab on a chip, integrated optics, microfluidics, femtosecond laser micromachining

1 | INTRODUCTION[1]

Drosophila Melanogaster, also known as fruit fly, is a widely recognized genetic model sharing about 75% of disease genes with humans. It is used as an animal model in biomedical research to study development, several pathologies, including cancer, congenital and aging syndromes, and rare diseases[1-3]. The high fertility, the ease of culturing and the short life cycle facilitate the study of large populations. As thoroughly discussed in recent reviews[4-7], microfluidics has been extensively used in combination with *Drosophila* analysis. Not only does it allow sample exposure to controlled environment conditions such as oxygen, chemicals, or temperature gradients[8-12], but it also does permit to increase the automation and the throughput of the measurements. In this regard, Chung et al. presented a PDMS microfluidic device with an embryo-trap array, used for parallelized imaging[13]. Shorr and co-workers studied the embryos response to mechanical stimulations, deforming the channels by the application of pressurized air[14]. Furlong, Chen and their respective colleagues, implemented high-throughput devices for the automatic sorting of embryos on chip [15,16]. Analogously, the field of microscopy has demonstrated an

[†] Roberto Memeo and Petra Paiè equally contributed to this work

increasing interest towards the continuous sample delivery offered by microfluidics[17]. Following this route, several groups worked towards the fabrication of advanced microscopes on chip (MOCs), based on different optical investigation techniques and microfluidic designs[18-20]. Beyond the device throughput, these MOCs present several advantages over bulk instrumentations, such as compactness, alignment stability, automation as well as reduced costs relative to advanced microscopes, which can usually be afforded by large facilities only. A technique that can highly benefit from automatic sample delivery is Light Sheet Fluorescence Microscopy (LSFM)[21-23]. In this technique, a plane of light illuminates a single cross section of the sample and the excited fluorescence is collected orthogonally by a microscope objective, forming an image of the section on the acquisition camera. This approach is characterized by high signal to noise ratio, low phototoxicity and fast sample acquisition. Specimens translation allows the illumination of the whole sample, plane by plane, and the acquisition of the stack of images necessary for 3D image reconstruction. Therefore, using LSFM it is possible to get volumetric information that are hard to discern with widefield microscopy. Nevertheless, the standard approach requires manual sample alignment and positioning, which limits the automation of this technique[21]. To address this potential bottleneck, several groups presented different solutions based on the synergy between microfluidics and LSFM[24]. Some implementations foresee the customization of LSFM setups to obtain compatibility with microfluidic devices[25-27]. For instance, McGorty et al. developed the Open-Top Microscope. Here, two microscope objectives, are positioned below the sample, mutually orthogonal, and used for sample illumination and collection[12,28]. To avoid the aberrations introduced when imaging at 45 degrees through a coverslip these authors used a water prism. Beyond the need of a custom setup, a main limitation of this approach is the requirement of a mechanical translation stage which entails unwanted vibration and alignment instability. Different solutions foresee a higher level of integration, using microfabricated prisms or mirrors[29]. For instance, Galland et al. developed a single objective LSFM, in which, thanks to a 45° tilted embedded micromirror, both sample illumination and detection are achieved through a single microscope objective[30]. This technique has been reproduced by different groups and combined with microfluidics for sample delivery[31]. This approach is compatible with standard inverted microscopes, but to achieve the whole sample scanning mechanical translation is still required. Miura et al. used an embedded micromirror to acquire images at a throughput comparable with the ones of conventional flow cytometers, benefitting from the higher signal to noise ratio that characterizes light sheet illumination with respect to widefield microscopy[32]. With their configuration a single plane per sample can be acquired. A different approach has been presented by Deschout et al. who generated light-sheet illumination on-chip through an integrated planar waveguide that faces a microchannel[33]. In this way, concentration retrieval of biomolecules has been demonstrated. One major drawback is the impossibility to acquire 3D images, as the fluid velocity direction lies in the same plane defined by the light sheet. In our group, taking advantage of the versatility of the used fabrication technique, Femtosecond Laser Micromachining (FLM), we have fabricated a light sheet-based microscope on-chip. In such approach, an integrated cylindrical lens focuses the light from a fiber in one direction, creating a light sheet that intercepts the microfluidic channel. We have demonstrated automatic optical sectioning of cellular spheroids, as well as of single cells, by using different lens profiles and light-sheet beam-waists[34,35]. By integrating the illumination on-chip, we have obtained compact and portable devices, characterized by a stable component alignment and compatible with standard widefield microscopes. In this work, we propose a new device layout, tailored to *Drosophila* embryos imaging. Indeed, these embryos are thick and elliptical in shape (they are approximately 500 μm long and 200 μm wide) and they must be correctly oriented with respect to the light sheet propagation direction in order to reduce the impact of aberrations in the acquired images. Scattering becomes more and more significant when imaging deep into the samples, limiting the capability of observing internal features of the specimens. Nevertheless, the ellipticity of *Drosophila* embryos turns in our favour once it can be controlled, since the orientation affects the maximum samples' thickness through which the images are acquired. We therefore designed and optimized an advanced fluidic layout for *Drosophila* embryos scanning that permits a controlled rotation of the samples during their flow. Furthermore, we used integrated waveguides for precise coupling and alignment of two counter-propagating light-sheets to evenly illuminate the entire sample. Here we describe how the optical and the fluidic elements have been synergistically engineered to be adapted for *Drosophila* automatic optical sectioning microscopy.

2 | EXPERIMENTAL

2.1 | Materials and methods

Fabrication technique

The fabrication technique used in this work is femtosecond laser micromachining. It is a versatile technique that allows to realise both optical and fluidic components in glass substrates with the desired 3D layout and with a maskless approach[36,37]. A pulsed laser beam is focused in a transparent substrate and, thanks to the high peak intensities, nonlinear absorption processes occur in the focal region, locally modifying the material. The localization of the induced modification is at the basis of the 3D capabilities of this technique. Indeed, sample translation permits to define three-dimensional patterns of modified material inside the substrate. The type of modification is highly dependent on the laser parameters. For instance, in fused silica glass it is possible to induce both a smooth refractive index increase and an enhanced etching selectivity. The first one allows for the formation of optical waveguides, while the latter permits to obtain microchannels by exposing the irradiated substrate to an etchant solution (typically hydrofluoric acid)[38-40]. The used laser source was a

commercial femtosecond laser system (Pharos, LIGHT CONVERSION), with an emission wavelength of 1028 nm and 1 MHz repetition rate. The laser beam was focused in a 3 mm thick fused silica substrate with a 50x, 0.65 NA microscope objective with correction ring (LCPLN 50XIR, Olympus). The sample was mounted on a three-dimensional translation stage (FIBERglide3D, Aerotech, Pittsburgh, PA, USA). We used different fabrication parameters for the microfluidic channels and the optical waveguides. Two sets of irradiation parameters were previously optimized to maximize, on the one side, the etching selectivity and, on the other, to reduce the waveguide losses. During the fabrication of the microfluidic channel, the translation speed and the laser pulse energy were set to 2 mm/s and 760 nJ, respectively, while the repetition rate was set to 500 kHz. To fabricate the microchannel, we irradiated several parallel lines that define the channel profile. The separation between subsequent laser scans was set to 5 µm for vertical planes and to 1 µm for horizontal surfaces. The microchannel spans through the whole height of the fabricated device (3 mm) and has a maximum cross section of 965 x 500 µm². Due to the large dimensions of the microchannel, we also irradiated multiple lines inside the volume of the structure (with a separation of 5 µm) to facilitate the chemical etching process. On the other hand, for optical waveguides fabrication, we used a translation speed and a pulse energy of 0.5 mm/s and 50 nJ respectively with a repetition rate of 50 kHz; waveguides were irradiated 750 µm deep from the substrate surface. Moreover, here we implemented a multi-scan approach[41], irradiating 7 parallel lines with a shift of 0.4 µm. This permitted to obtain a square cross section of the modified region with final dimensions of 3.5 µm x 3 µm and a uniform refractive index modification. We characterized the waveguides properties for both blue and green light. In detail, we have estimated propagation losses equal to 0.26 dB/cm and a mode diameter equal to 6 x 6.5 μm^2 for green light (561 nm). Whereas, we have estimated 0.08 dB/cm and a mode diameter of 4.2 x 4 μm^2 for blue light (488 nm). The induced refractive index contrast was estimated by means of a numerical simulation aiming at matching the calculated guided mode with the experimental one. This procedure gives an estimation of the obtained index contrast (with respect to the pristine material), being equal to $3.5 \cdot 10^{-3}$ and $6.5 \cdot 10^{-3}$ for green and blue light, respectively. After the irradiation step, the glass substrates were exposed to an aqueous solution of hydrofluoric acid (HF at 20%) in a sonic bath at 35°C. The irradiation and the etching processes lasted approximately 10 and 7 hours, respectively. Subsequently, the substrates were polished to optical quality and the waveguides were fiber pigtailed. As illustrated in Figure 1 and in Figure 2, to favour the sample delivery, we have inserted a pipette tip in the microfluidic inlet, while we have inserted a PEEK (PolyEtherEtherKetone) tube in the microchannel outlet (UpChurch Scientific, catalogue #1569). Both the pipette tip and the PEEK tube have been glued to the substrate using a curable resin (DELO- Photobond GB345). By connecting the tube to a syringe pump (KDS410, from KDScientific, Holliston MA, USA) in withdrawal mode, we could precisely control the sample movement through the chip. During image acquisition the fluidic system was set on a flow rate of 2 ml/h.

Biological samples preparation

Drosophila flies were maintained in dedicated incubators at 25°C. Embryos collection was performed using air-permeable cages with removable bottom plates for egg collection. Due to the continuous egg deposition, plates were changed every day, and embryos were collected and processed within 24 hours from deposition to prevent hatching into larvae. Collected embryos were subsequently fixed for 20 minutes using a solution of 4% Paraformaldehyde (PFA) in PEM (0.1M PIPES, 1mM MgCl2, 1mM EGTA, pH 6.9). With this procedure, embryos can be stored for months at -32°C. In this work, we have processed embryos populations of two genotypes encoding fluorescent proteins. The first one expressing cytoplasmic GFP ubiquitously (Act5C-GAL4, UAS-GFP courtesy of D. Grifoni, Università di Bologna) and the second expressing RFP in nuclei of all cells (w-; His2av-mRFP1; BDSC stock 23651). During device validation experiments, the embryos were diluted in a liquid suspension of water and 0.1% agar, to prevent them from freely sinking in the liquid solution: they can thus be approximated as neutrally buoyant. Different agar concentrations were experimentally tested, and we found 0.1% to be the optimum concentration.

Integrated light sheet microscopy setup

The compactness and portability of our device make it highly compatible with standard fluorescence microscopes, which can be upgraded with our chip for 3D fluorescence image reconstruction of the samples. In this work, we have mounted the chip on a custom-made inverted microscope to further increase the system compactness and simplicity (as in Figure 1). Images are acquired with a 20x, 0.45NA microscope objective lens with a correction ring for up to 2 mm of glass (CFI S Plan Fluor ELWD 20X, Nikon).

The objective lens was at focus on the excitation plane created by the light sheet in the chip. The fluorescence signal collected by the objective was filtered with a dual band filter (Semrock FF01-512/630-25) and focused through a tube lens (Olympus U-TV1XC) on a high speed CMOS camera (Hamamatsu Orca Flash 4.0 V3), which acquires images with

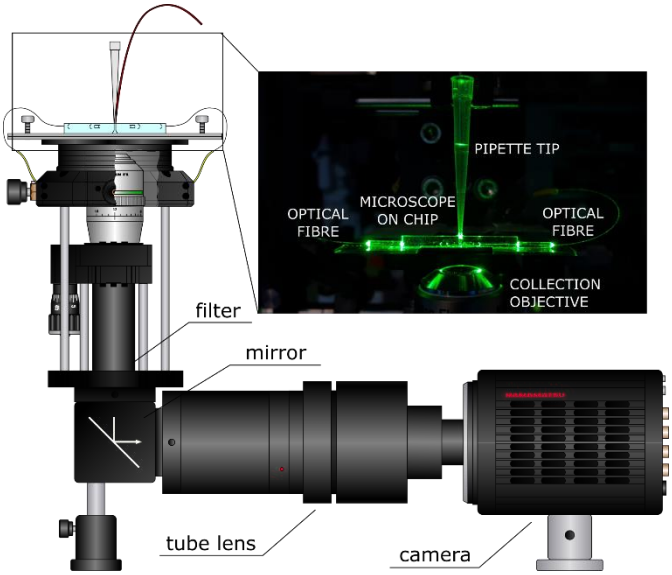

Figure 1. Scheme of the custom microscope used for image acquisition.

a maximum frame rate of 100 Hz. Two different laser sources (OBIS, Coherent) with emission wavelengths of 488 and 561 nm were alternately coupled to the chip to excite the fluorescent proteins expressed by the samples. Potentially, simultaneous acquisition of two-color images can be implemented by using a wavelength division multiplexer (WDM) and alternating the two laser lights in synchrony with the camera acquisition rate.

2.2. New Chip Development

Schematic device layout

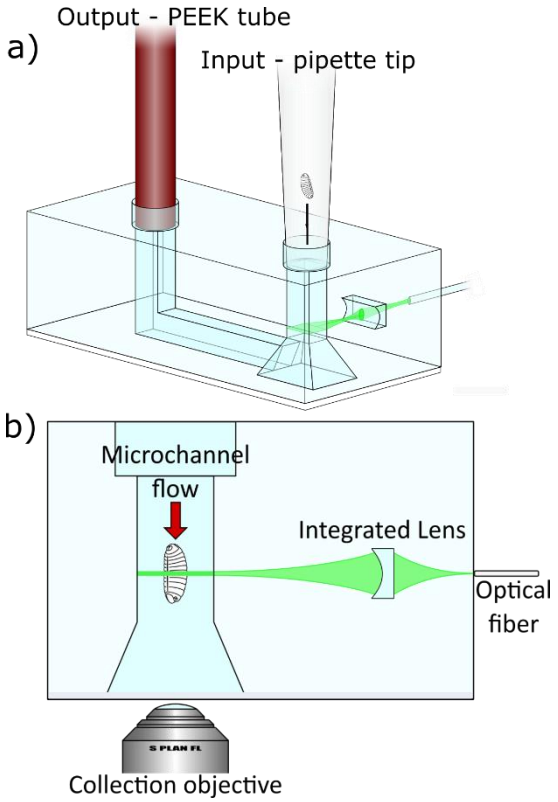

Figure 2. Schematic of the basic working principles of the microscope on chip. Panel a) and b) illustrate the 3D and the front view of the device, respectively.

The schematic design of the device is reported in Figure 2.a. As illustrated, while flowing in the microfluidic channel from inlet to outlet, the specimens are automatically sectioned by the light sheet generated by an integrated cylindrical lens. The images were acquired orthogonally by an external widefield microscope, as shown in Figure 2.b. The acquisition of the fluorescence signal emitted by all the planes in which the specimen is divided allows for its full 3D reconstruction. The bottom tapering of the channel is introduced to reduce the impact of image aberrations due to the presence of the lateral side walls of the channel. The tapering is designed to fit the numerical aperture of the microscope objective used to collect the images. In addition, we had to address the challenges related to the shape and dimensions of the embryos. A first problem is represented by the fact that the images are acquired through the embryos themselves. Thus, at the beginning of the sample sectioning, the images look sharper as they are not imaged through the turbid media of the embryo itself. Then, they become more and more blurred during the acquisition, as the images are acquired deep into the specimens. This is particularly accentuated when the embryos are flowing oriented parallel to the flow velocity direction, as schematically shown in Figure 2.b and in supplementary Figure S1. Considering the ellipticity of the embryos, the impact of this problem is reduced when the specimens are flowing with their major axis oriented perpendicularly to the flow. Therefore, we decided to implement a solution to address an automatic horizontal orientation of the samples. A second issue is that these samples are quite thick and scattering, therefore they could affect the quality of the light sheet. To guarantee a more uniform illumination over the sample we decided to introduce a dual-side illumination, whose precise alignment is guaranteed by the use of integrated waveguides, in place of optical fibers.

Automatic sample orientation

Elliptical particles in Stokes flow can be oriented with their main axis along the flow direction or undergo an uncontrolled rotation depending on their initial orientation and on the flow rate value[42]. Both events are unwanted for our applications. Indeed, an uncontrolled rotation does not permit the correct 3D volumetric evaluation, while the vertical orientation of the embryo (Figure 2.b), is the configuration where the image quality is mainly affected by scattering (see also Figure S1 and discussion in the previous section). Experimentally, we

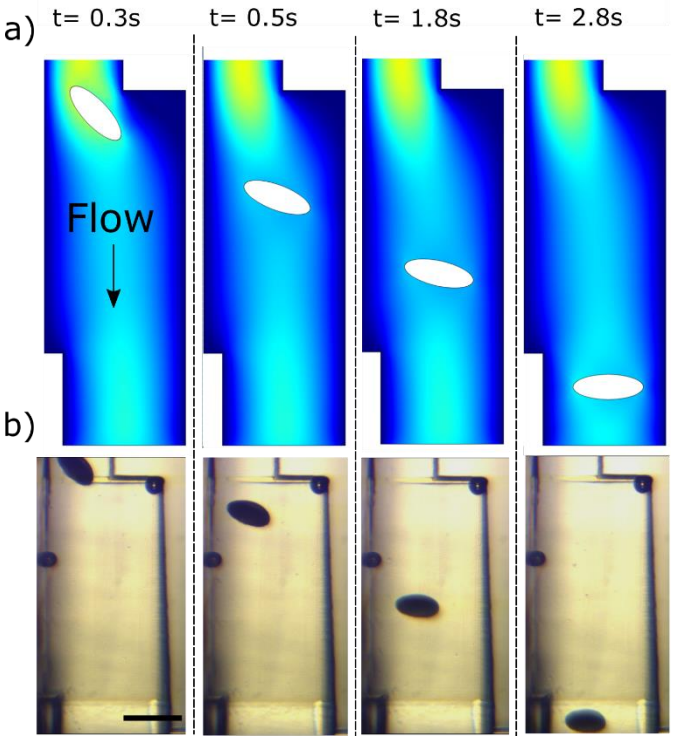

Figure 3. Panel a) shows a COMSOL simulation of the specimen rotation induced at a flow rate of 2 ml/h, while panel b) shows the corresponding device validation with a *Drosophila* embryo. Note that the simulated and fabricated devices have the same dimensions. Scale bar is 500 µm.

have observed that in our device this circumstance is the most frequent (see MOVIE_01).

To avoid this problem, we have decided to optimize the layout of the microfluidic channel, performing a passive and automatic sample orientation. In literature, there are several works that deal with particle orientation in microfluidics[42-44]. Most of them require active forces or flow rates which are incompatible with our application. Here we present a microfluidic module that passively induces a controlled embryo rotation, without the need of multiple inlets or external active fields. To achieve full compatibility, with LSFM we set the flow rate to 2 ml/h, which allows a good balance between the number of acquired planes per sample and the total acquisition time. Therefore, we modified the microchannel layout introducing an expansion chamber to asymmetrical bend the fluid velocity profile, as illustrated in Figure 3, while Figure S2 shows the entire profile of the optimized microchannel. We have optimized this layout by means of numerical simulations carried out in COMSOL Multiphysics (Burlington, MA, USA). In particular, taking advantage of the fluid-solid interaction module provided by the software, we have explored the microchannel dimensions that would allow to achieve the desired sample rotation (see Figure S3). As a final step, we have experimentally validated the numerical simulations, fabricating a device with the previously optimized dimensions. From the side view inspection of many samples flowing inside the microfluidic channel (see MOVIE_01), we have retrieved the rotation efficiency as the number of embryos correctly rotated over the total number of processed specimens. We have set the acceptance threshold to 45°, which indicates the maximum inclination with respect to the horizontal orientation that allows to consider an embryo as correctly rotated. This value was chosen as it represents the limit between the two rotated/unrotated positions and it still allows to obtain a good image quality. Under this condition, we counted that 79 over 93 embryos were correctly rotated, which corresponds to 85% rotation efficiency. While, reducing the threshold to an inclination of 15°, the measured efficiency is 61% (57 over 93 embryos). Without the microfluidic optimization almost all of them remained oriented parallel to the flow velocity direction. A direct comparison between experimental validation and simulations is reported in Figure 3 and MOVIE_02.

Dual-sided illumination

To implement dual-side illumination, a first approach would be to simply add to the device layout illustrated in Figure 2 a second lens symmetrically placed with respect to the microfluidic channel. This, in turn, would focus the light from a second optical fiber into the channel, generating a light sheet perfectly overlapped with the first one. Anyway, this approach does not take into consideration the possible misalignment between the two optical fibers. This could generate a thick and uneven light sheet, highly decreasing the quality of the acquired images and the optical sectioning

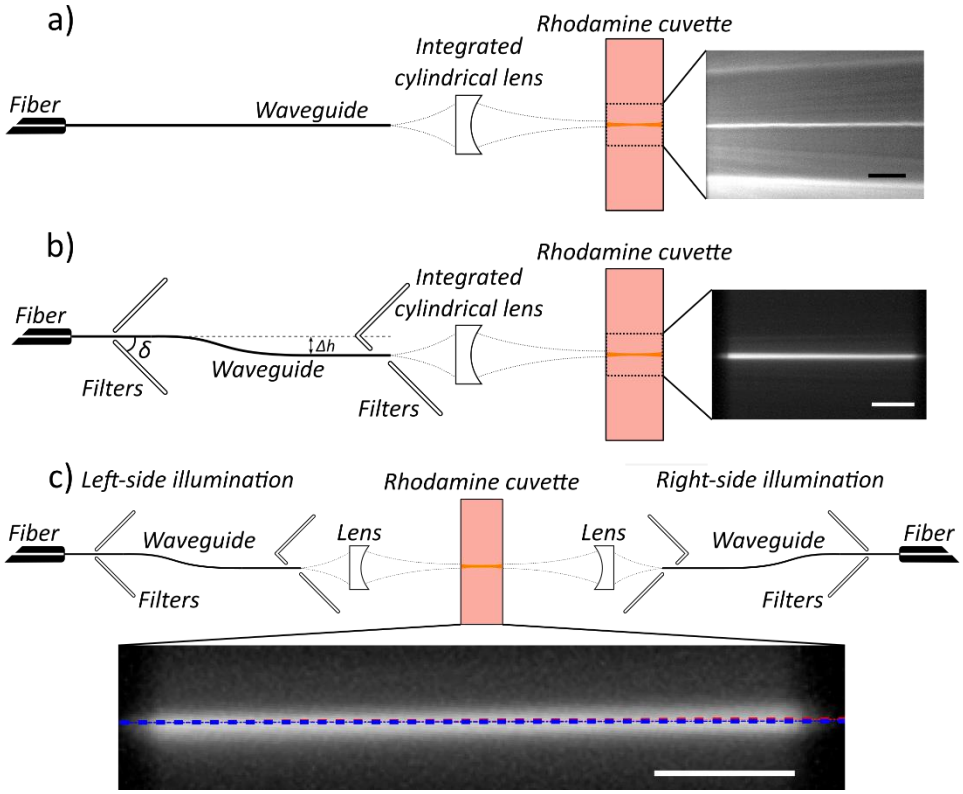

Figure 4. Schematic illustration of the different devices used to test the optical properties of the integrated microscope with the corresponding experimental result. In panel a) the light from an integrated optical waveguide is focused in the Rhodamine cuvette. In panel b) stray light filters are introduced and the waveguide is bent to increase the signal to noise ratio. Panel c) shows the device used to analyse the dual side illumination capability. Scale bars are 100 µm.

capabilities. To avoid this problem, we decided to take advantage of the capabilities of femtosecond laser micromachining. Therefore, we directly wrote two opposite optical waveguides in the same irradiation process. Considering that all the integrated components (optical and fluidics) are fabricated by laser irradiation in a single step, the alignment between them is guaranteed with a precision of 100 nm.

We started from the characterization of a single light sheet, obtained by focusing the light coming from one optical waveguide by means of an integrated cylindrical lens. In this work we have decided to use an empty plano-concave lens. This consists in a cylindrical hole fabricated in the fused silica substrate by femtosecond laser micromachining, as illustrated in Figure S4. The lens profile, as discussed in supplementary material, is optimized to obtain a light sheet with a waist of about 7 µm, which guarantees a uniform illumination over the whole sample channel. To characterize the optical properties of the light sheet, we have fabricated an integrated cuvette in front of the lens, in correspondence of the expected position of the focused light sheet as illustrated in Figure 4. The dimensions of the cuvette are 2x1x0.5 mm^3, where 0.5 mm is the length along the beam propagation direction, to simulate the dimensions of the microfluidic sample channel. Subsequently, we filled the cuvette with Rhodamine. The analysis of the Rhodamine fluorescence excited by the light sheet allows one to determine the lens optical properties. From this characterization, as shown in Figure 4.a, we observed that the light sheet is correctly created inside the Rhodamine cuvette.

Nevertheless, it is possible to note the presence of a strong background. We measured a signal to noise ratio of 2.5. This is due to the light from the fiber that is not coupled to the waveguide and that diverges through the substrate creating the fluorescence background. This background spoils the quality of LSFM images. To avoid it, we decided to fabricate a set of integrated stray light filters. We created these components as hollow slots that back reflect light thanks to total internal reflections. The angle between the straight waveguide direction and the stray light filter (δ) was chosen to allow total internal reflection of the uncoupled light. Moreover, to maximize the background reduction, the waveguide was written with a slight S-bend. This created a misalignment (Δh = 100 µm) between the fiber direction and the aperture gap between stray light filters, thus enhancing the filtering capabilities. The schematic design of the device and its characterization is illustrated in Figure 4.b. Here, it is possible to observe that the background is strongly reduced, with a measured signal to noise ratio of 7.

Subsequently, we have investigated the possibility of performing dual-sided illumination by overlapping two opposite light-sheets. To perform this measurement, we have fabricated a new device in which two opposite waveguides are facing a single cuvette, as illustrated in Figure 4.c; both waveguides have been fiber pigtailed.

First, we have acquired the images of the two obtained light-sheets by illuminating from each side. Then, we simultaneously illuminated the integrated cuvette from both sides and we have analysed the images. We have then retrieved that the two light sheets generated by the counterpropagating focused beams are well overlapped (as indicated in Figure 4.c by the blue and red dotted lines which identify the central position of each light sheet). We measured an average separation between the two beams of about 0.7 µm, which has a limited impact on our sectioning capabilities, considering the width of the single light sheet.

Device characterization

Combining the results obtained in the fluidic and optical components optimization, we fabricated the final device, in which the microfluidic sample channel is symmetrically illuminated by two counter-propagating light sheets. The total dimensions of the on-chip microscope are 32x5.8x3 mm^3, which underlines the compactness of the platform. The complete scheme of the device is illustrated in Figure 5. The device was subsequently fiber-pigtailed with two optical fibers and fluidically connectorized by inserting the PEEK tube and the pipette tip. To characterize the microscope axial resolution we measured the light-sheet thickness. To do so, we filled the sample channel with Rhodamine and we placed the device 90° tilted under a standard fluorescence microscope so that the light sheet profile was clearly visible. Indeed, by analysing the images with a Gaussian fit we could retrieve the beam waist dimension and position[45]. Images of fluorescence excitation were acquired with both single and dual sided illumination for each wavelength. The measured beam waists obtained by dual sided illumination are 4.9 ± 0.14 µm and 5.9 ± 0.76 µm, for blue and green light, respectively, as illustrated in Figure S5. These values are in good agreement with the designed ones, which allows a good

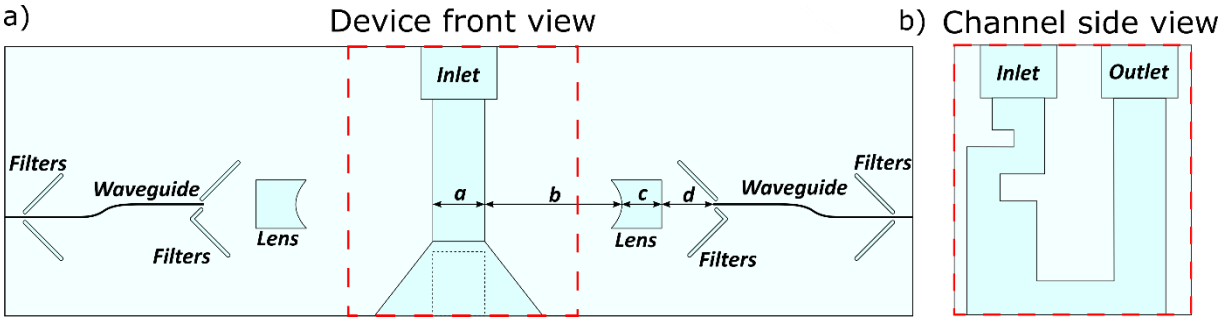

Figure 5. Schematic design of the final device. Panel a) shows the front view of the microscope on chip (not in scale). The dimensions of a, b, c and d are 500 µm, 4.5 mm, 800 µm, 1 mm, respectively. Panel b) illustrates the side view of the microfluidic channel, with the profile optimized for automatic sample rotation.

optical sectioning
This result proves the possibility to use the same microscope on chip for dual color illumination, due to the similar illumination conditions at the different wavelengths. Subsequently, we mounted the device in the custom inverted microscope (as in Figure 6). The image quality was analysed by flowing in the device fluorescent nanobeads from Phosphorex (diluted in a liquid solution of water and agar) with an average diameter of 100 nm, at a controlled flow rate. Through the analysis of the FWHM of the point spread function of different beads we were able to retrieve the lateral resolution of the system (Figure S6 and Table S1).

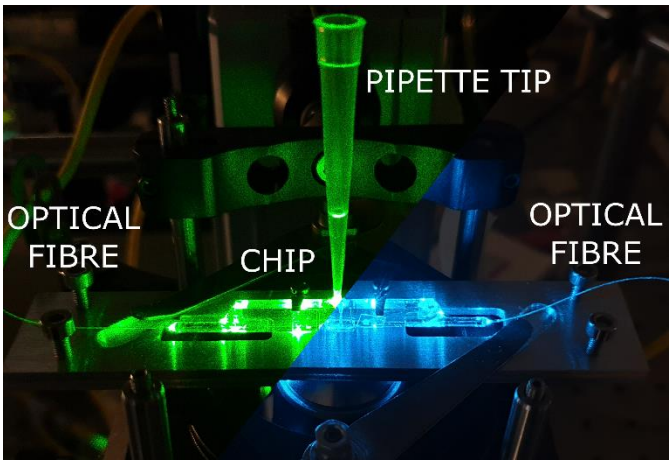

Figure 6. Final device assembled and mounted in the custom set up used for sample image acquisition. The figure is obtained merging two pictures acquired switching the laser light.

We measured an averaged lateral resolution of about 0.99 and 1.05 μm, while the theoretical achievable limits are 0.72 and 0.83 μm for the two illumination wavelengths: 488 nm and 561 nm, respectively. This discrepancy is probably due to the presence of residual spherical aberrations, along the detection arm. Indeed, we are acquiring images through a glass slab, deep into a microfluidic channel filled with an aqueous solution of agar, whereas the microscope objective compensation is intended only for the glass slide.

3 | RESULTS AND DISCUSSIONS

Imaging of *Drosophila* embryos
We started the device validation with analysing the sample population expressing GFP, thus we excited the samples using a 488 nm laser. Figure 7 shows an example of the acquired images. In detail, panel a) shows the Maximum Intensity Projection (MIP) obtained using the acquired stack of images, while panel b) shows a single plane from the same specimen. It is worth noting that an almost uniform illumination over the whole sample is achieved. Panel c) shows different sections of the sample acquired while the embryo is flowing through the light sheet (see also MOVIE_03).
The presented planes are separated by 25 μm steps. Thanks to the optical sectioning capabilities, from these images it is possible to retrieve information of the inner structure of the embryo. In Figure 7d, a detail of the developing gut is presented, showing that resolution of a tissue monolayer can be achieved with the device. The time required to process a single specimen is typically 0.8 s. Therefore, with this device we can automatically process a large number of samples. The specimens acquisition rate depends on the sample concentration in the liquid solution, with an upper limit of 75 specimens/minute, due to the time needed to acquire the images from a single specimen. To avoid any risk of clogging the channel due to the large dimensions of the embryos we preferred to work with a diluted solution, processing them

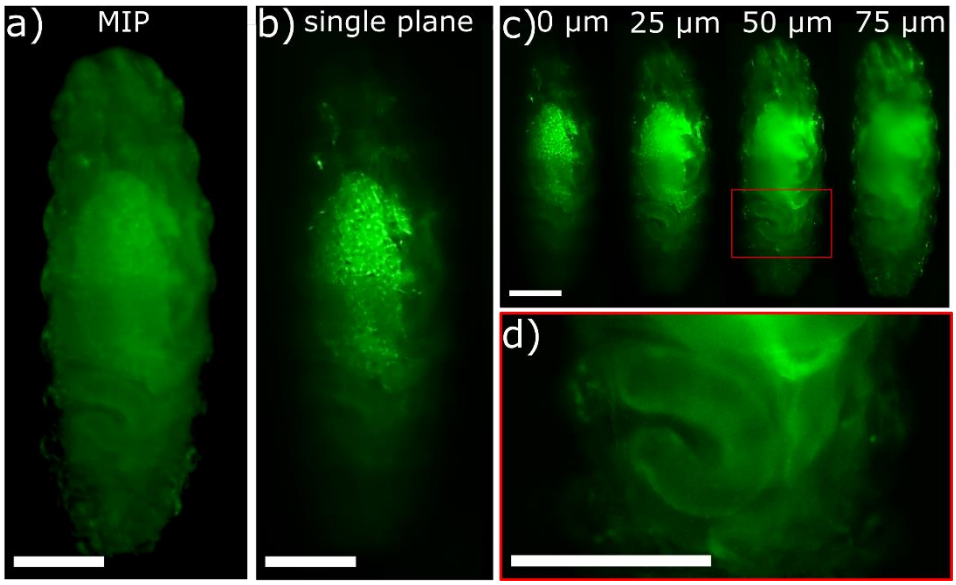

Figure 7. Panel a) shows the Maximum Intensity Projection (MIP) of a stage 17 *Drosophila* embryo (head side up, dorsal view). Panel b) shows a single section of the same specimen showing the surface. Panel c) shows sections of the embryo at different depths, acquired during the sample movement through the light sheet. In panel d) a detail of the region highlighted in red is reported, showing a detail of the looping midgut. Scalebar is 100 μm.

with a maximum rate of 20 samples/minute.

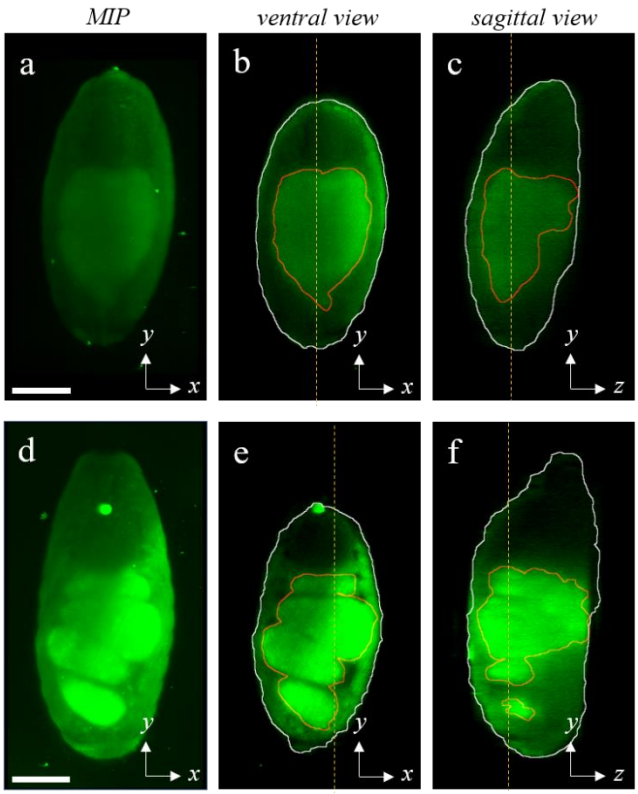

Figure 8. Panels a) and d): maximum intensity projection of embryos of two consecutive stages (head side up, ventral view). Panel a): stage 15, characterized by a heart-shaped midgut. Panel d): stage 16, with the 4 midgut compartments separated by 3 midgut constrictions. Panels b) c), e) and f): corresponding ventral and sagittal views. Scalebar is 100 μm.

This is a significant result considering that bulk LSFM systems require up to several minutes for manual positioning and alignment of a single sample. The device allows for 3D observation of the internal organs, segmentation and quantification of their volumes. This can be used to identify different developmental stages based on quantitative differences in morphology. An example is presented in Figure 8, in which Act5C-GAL4, UAS-GFP embryos are sectioned in perpendicular orientations. Since the GFP is expressed under control of the actin promoter, we observe a high fluorescence signal in the internal organs and specifically in the actin-rich muscle surrounding the gut. Thus, the high signal that reveals the fine shape of the midgut can be used to precisely determine the developmental stage of the imaged embryo. In particular, a typical heart-shaped midgut is visible in Figure 8a-c indicating that the upper embryo is at stage 15. The midgut shown in Figure 8d-f presents 4 folded chambers, indicating that the embryo is at stage 16. The external volume of the embryo can be segmented using a simple threshold while the segmentation of the midgut requires a more advanced thresholding method. We have applied an adaptive threshold and processed the stack plane by plane using the Python module open-cv, but a further manual adjustment of the volume border was required for this dataset. The fluorescence intensity in the midgut shows a 2.5-fold increase from stage 15 to 16 embryos of Figure 8, which could be used to automatically assign the developmental stage.

In a different experiment, we tested the device with a population of *Drosophila* embryos expressing ubiquitously nuclear mRFP. In this case we investigated the sample properties using an excitation laser at 561 nm. The measurement could be performed at this wavelength thanks to the small chromatic differences in the light sheet properties between the blue and green excitation. Figure 9 shows a single plane acquired in three different specimens expressing RFP. It is possible to observe and clearly recognize the internal structure of the embryos at near-single cell resolution, despite their thickness and optical density.

In both the experiments, we observe that the internal features of the embryo are visible, and this information can be used for the identification of different stages or phenotypes. This paves the way to automatic recognition of the development traits, which could be based not only on the measurement of the fluorescence intensity, but also on advanced volumetric segmentation and unsupervised classification of the embryo anatomy.

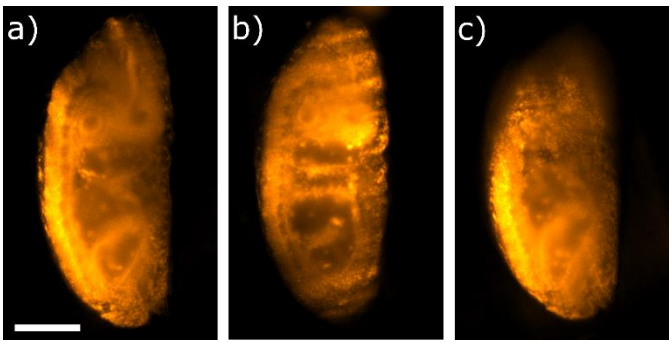

Figure 9. Single plane acquisitions of 3 different embryos at stage 14-15 (head side up, lateral view) whose nuclei are marked by RFP. The ventral nerve cord is visible on the left side of the embryo (a), the more superficial body segments are recognizable (b), or head structures are highlighted (c). Scale bar is 100 μm.

4 | CONCLUSIONS

In this work we have presented a new microscope on chip, specifically developed for automatic imaging of *Drosophila* embryos. This compact and portable device was fabricated by combining optical and fluidic components, which have been carefully optimized to allow the generation and overlap of two light sheets in a fluidic channel. We have designed and optimized the fluidic system to automatically align *Drosophila* embryos and we processed two different populations expressing GFP and mRFP, respectively. The obtained results show good volumetric reconstruction of samples flowing through the light sheet in less than a second, proving the capability to perform automatic light sheet microscopy, at two different wavelengths. Embryonic, developmental stages, tissues and, in some cases, single cells were clearly visible. While discrimination of the different

stages might heavily depend on levels of the fluorophores of interest, our set up could be used to analyse systematically patterns of mRNA or protein expression and localization, or mutant phenotypes including identification of rare variants. In particular, when associated to real-time quantification of florescence signal, it is envisaged that the system could be applied to counting embryos belonging to a particular stage or displaying a particular pattern or phenotype. A further coupling to a sorting device as in Furlong et al. (2001) and in other, more recent, works[15,46,47], would allow recovery and subsequent analyses, or culturing, of embryos with defined, quantitative traits, based on up to 2 colour parameters. Potential applications of such an integrated system would include -omics approaches applied to rare population of embryos, for example to understand mechanisms of genetic variability underlying quantitative traits.

ACKNOWLEDGEMENT

The authors would like to acknowledge Roberta Mazzoleni for her preliminary activity on the fabrication of integrated optical components and Antonio Galeone for help in interpreting image data.
This work was supported by the PROCHIP Project, a FET Open project granted by European Union (grant ID: 801336) to F.B., LASERLAB-EUROPE (grant ID: 871124, European Union's Horizon 2020 research and innovation programme) to A.B, and by AIRC (grant ID: 20661) and WCR (grant ID: 18-0399) to T.V.

AUTHOR CONTRIBUTION

TV, AB, RO, PP and FB conceived the experiments. RM, PP and FB designed the device. RM and CG prepared and collected the biological samples. AB, MC and FS optimized the setup and the device interfaces. RM and PP fabricated and validated the device. AB performed the images postprocessing. All the authors discussed the results and contributed to the manuscript preparation.

CONFLICTS OF INTEREST

There are no conflicts to declare.

DATA AVAILABILITY STATEMENT

All data needed to support the conclusions of the paper are present in the paper and/or the Supplementary Materials. The original stacks of images as well as the custom software for lens optimization may be requested to the authors.

NOTES AND REFERENCES

1 E. Bier, *Nat. Rev. Genet*, **2005**, 6(1), 9-23.
2 M.D. Adams, S.E. Celniker, and R.A. Holt, *Science*, **2000**, 287(5461), 2185-95.
3 M. Mavrakis, R. Rikhy, M. Lilly and J. Lippincott-Schwartz, *Curr Protoc Cell Biol.*, **2008**, 39(1), 4-18.
4 A. Zabihihesari, A.J. Hilliker, and P. Rezai, *Integr. Biology*, **2019**, 11(12), 425-443.
5 B. Lin, and A. Levchenko, Frontiers in bioengineering and biotechnology, **2015**, 3, 39.
6 H. Hwang, and H. Lu, Biotechnol. J., **2013**, 8(2), 192-205.
7 V. Sivagnanam, and M.A. Gijs, *Chem. Rev.*, **2013**, 113(5), 3214-3247.
8 E.M. Lucchetta, M.S. Munson, and R.F. Ismagilov, *Lab Chip*, **2006**, 6(2), 185-190.
9 G.T. Dagani, K. Monzo, J.R. Fakhoury, C.C. Chen, J.C. Sisson, and X. Zhang, *Biomed. Microdevices*, **2007**, 9(5), 681-694.
10 Z. Wang, S.C. Oppegard, D.T. Eddington, and J. Cheng, *PloS One*, **2017**, 12(9).
11 T.J. Levario, C. Zhao, T. Rouse, S.Y. Shvartsman and H. Lu, *Sci. Rep*., **2016**, 6, 21366.
12 R. McGorty, H. Liu, D. Kamiyama, Z. Dong, S. Guo, and B. Huang, *Opt. Express*, **2015**, 23(12), 16142-16153.
13 K. Chung, Y. Kim, J.S. Kanodia, E. Gong, S.V. Shvartsman, and H. Lu, Nature methods, **2011**, 8(2), 171-176.
14 A.Z. Shorr, U.M. Sönmez, J.S. Minden, and P.R. LeDuc, *Lab Chip*, **2019**, 19(7), 1141-1152.
15 E.E. Furlong, D. Profitt, and M.P. Scott, *Nat. Biotechnol*. **2001**, 19(2), 153-156.
16 C.C. Chen, S. Zappe, O. Sahin, X.J. Zhang, M. Fish, M. Scott, and O. Solgaard, *Sens. Actuators B Chem*, **2004**, 102(1), 59-66.
17 P. Paiè, R.M. Vázquez, R. Osellame, F. Bragheri and A. Bassi, *Cytometry A*, **2018**, 93(10), 987-96.
18 X. Cui, L.M. Lee, X. Heng, W. Zhong, P.W. Sternberg, D. Psaltis, and C. Yang *Proc. Natl. Acad. Sci. USA*, **2008**, 105,10670–10675.
19 W. Bishara, H. Zhum, A. Ozcan, *Opt. Express*, **2010**, 18,27499–27510.
20 V. Bianco, B. Mandracchia, V. Marchesano, V. Pagliarulo, F. Olivieri, S. Coppola, M. Paturzo, and P. Ferraro, *Light Sci. App*., **2017**, 6(9), e17055-e17055.
21 J. Huisken, J. Swoger, F. Del Bene, J. Wittbrodt and E. H. Stelzer, *Science*, **2004**, 305, 1007.
22 E.G. Reynaud, U. Kržič, K. Greger and E.H.K. Stelzer, *HFSP Journal*, **2008**, 2(5), 266–275.
23 A. Costa, A. Candeo, L. Fieramonti, G. Valentini and A. Bassi, *PLoS One*, **2013**, 8.
24 I. Albert-Smet, A. Marcos-Vidal, J.J. Vaquero, M. Desco, A. Muñoz-Barrutia, and J. Ripoll, *Front. Neuroanat*., **2019**, 13, 1.
25 J. Wu, J. Li, and R.K. Chan, *Opt. Express*, 2013, 21(12), 14474-14480.
26 C.K. Rasmi, S. Padmanabhan, K. Shirlekar, K. Rajan, R. Manjithaya, V. Singh, and P.P. Mondal, *Appl. Phys. Lett.*, **2017**, 111(24), 243702.
27 H. Jiang, Z. Tingting, Z. Hao, N. Jun, G. Zeyi, H. Chi-Ming, L. Sheng, and F. Peng, *Lab Chip*, **2017**, 17(13), 2193-2197.
28 R. McGorty, D. Xie, and B. Huang, *Opt. Express*, **2017**, 25(15), 17798-17810.
29 F. Greiss, M. Deligiannaki, C. Jung, U. Gaul, and D. Braun, *Biophys. Journal*, **2016**, 110(4), 939-946.
30 R. Galland, G. Grenci, A. Aravind, V. Viasnoff, V. Studer, and J.B. Sibarita, *Nat. Methods*, **2015**, 12(7), 641-644.
31 M.B. Meddens, et al. *Biomed. Opt. Express*, **2016**, 7(6), 2219-2236.
32 T. Miura, H. Mikami, A. Isozaki, T. Ito, Y. Ozeki, and K. Goda, *Biomed. Opt. Express*, **2018**, 9(7), 3424-3433.

33 H. Deschout, F.C. Zanacchi, M. Mlodzianoski, A. Diaspro, J. Bewersdorf, S.T. Hess, and K. Braeckmans, *Nat. Methods*, **2014**, 11(3), 253.
34 P. Paiè, F. Bragheri, A. Bassi and R. Osellame, *Lab Chip*, **2016**, 16(9), 1556-60.
35 F. Sala, M. Castriotta, P. Paiè, A. Farina, S. D'Annunzio, A. Zippo, R. Osellame, F. Bragheri and A. Bassi, *Biomed. Opt. Express*, **2020**, 11(8), 4397-4407
36 R. Gattass and E. Mazur, *Nat. Photonics*, **2008**, 2, 219
37 R. Osellame, H. J. Hoekstra, G. Cerullo and M. Pollnau, *Laser Photonics Rev*., **2011**, 5, 442.
38 P. Paiè, F. Bragheri, R.M. Vazquez and R. Osellame, *Lab Chip*. **2014**, 14(11), 1826-33.
39 A. Schaap, Y. Bellouard, and T. Rohrlack, *Biomed. Opt. Express*, **2011**, 2(3), 658-64.
40 L. Qiao, F. He, C. Wang, Y. Cheng, K. Sugioka, and K. Midorikawa, Applied Physics A, **2011**, 102(1), pp.179-183.
41 Y. Nasu, M. Kohtoku and Y. Hibino, *Opt. Lett*., **2005**, 30(7), 723-5.
42 M. Li, H.E. Muñoz, A. Schmidt, B. Guo, C. Lei, K. Goda, and D. Di Carlo, *Lab Chip*, **2016**, 16(22), 4458-4465.
43 A. Ozcelik, N. Nama, P.H. Huang, M. Kaynak, M.R. McReynolds, W. Hanna-Rose, and T.J. Huang, *Small*, **2016**, 12(37), 5120-5125.
44 T. Cacace, P. Memmolo, M.M. Villone, M. De Corato, M. Mugnano, M. Paturzo, P. Ferraro, and P.L. Maffettone, *Lab Chip*, **2019**, 19(18), 3123-3132
45 P. Paiè, F. Bragheri, T. Claude and R. Osellame, *Opt. Express*, **2017**, 25(7), 7313-23.
46 F. Bragheri, P, Minzioni, R. Martinez-Vazquez, N. Bellini, P. Paiè, C. Mondello, R. Ramponi, I. Cristiani, and R. Osellame, *Lab Chip*, **2012**, 12(19), pp.3779-3784.
47 R. Utharala, Q. Tseng, E.E. Furlong and C.A. Merten, *Anal. Chem*., **2018**, 90(10):5982-8.

SUPPORTING INFORMATION

Additional Supporting Information may be found online in the supporting information tab for this article.